AMERICAN SOCIETY FOR MICROBIOLOGY | mBio®

RESEARCH ARTICLE
Therapeutics and Prevention

Deciphering the Evolution of Cephalosporin Resistance to Ceftolozane-Tazobactam in *Pseudomonas aeruginosa*

Melissa D. Barnes,[a,b] Magdalena A. Taracila,[a,b] Joseph D. Rutter,[a] Christopher R. Bethel,[a] Ioannis Galdadas,[i] Andrea M. Hujer,[a,b] Emilia Caselli,[g] Fabio Prati,[g] John P. Dekker,[h] Krisztina M. Papp-Wallace,[a,b,e,f] Shozeb Haider,[i] Robert A. Bonomo[a,b,c,d,e,f,j,k]

[a]Research Service, Louis Stokes Cleveland Department of Veterans Affairs, Cleveland, Ohio, USA
[b]Department of Medicine, Case Western Reserve University, Cleveland, Ohio, USA
[c]Department of Molecular Biology and Microbiology, Case Western Reserve University, Cleveland, Ohio, USA
[d]Department of Pharmacology, Case Western Reserve University, Cleveland, Ohio, USA
[e]Department of Biochemistry, Case Western Reserve University, Cleveland, Ohio, USA
[f]Department of Proteomics and Bioinformatics, Case Western Reserve University, Cleveland, Ohio, USA
[g]Department of Life Science, University of Modena and Reggio Emilia, Modena, Italy
[h]Department of Laboratory Medicine, Clinical Center, Microbiology Service, National Institutes of Health, Bethesda, Maryland, USA
[i]UCL School of Pharmacy, University College London, London, United Kingdom
[j]CWRU-Cleveland VAMC Center for Antimicrobial Resistance and Epidemiology (Case VA CARES), Cleveland, Ohio, USA
[k]Geriatric Research Education and Clinical Centers (GRECC), Louis Stokes Cleveland Department of Veterans Affairs, Cleveland, Ohio, USA

ABSTRACT *Pseudomonas aeruginosa* produces a class C β-lactamase (e.g., PDC-3) that robustly hydrolyzes early generation cephalosporins often at the diffusion limit; therefore, bacteria possessing these β-lactamases are resistant to many β-lactam antibiotics. In response to this significant clinical threat, ceftolozane, a 3′ aminopyrazolium cephalosporin, was developed. Combined with tazobactam, ceftolozane promised to be effective against multidrug-resistant *P. aeruginosa*. Alarmingly, Ω-loop variants of the PDC β-lactamase (V213A, G216R, E221K, E221G, and Y223H) were identified in ceftolozane/tazobactam-resistant *P. aeruginosa* clinical isolates. Herein, we demonstrate that the *Escherichia coli* strain expressing the E221K variant of PDC-3 had the highest minimum inhibitory concentrations (MICs) against a panel of β-lactam antibiotics, including ceftolozane and ceftazidime, a cephalosporin that differs in structure largely in the R2 side chain. The k_{cat} values of the E221K variant for both substrates were equivalent, whereas the K_m for ceftolozane (341 ± 64 μM) was higher than that for ceftazidime (174 ± 20 μM). Timed mass spectrometry, thermal stability, and equilibrium unfolding studies revealed key mechanistic insights. Enhanced sampling molecular dynamics simulations identified conformational changes in the E221K variant Ω-loop, where a hidden pocket adjacent to the catalytic site opens and stabilizes ceftolozane for efficient hydrolysis. Encouragingly, the diazabicyclooctane β-lactamase inhibitor avibactam restored susceptibility to ceftolozane and ceftazidime in cells producing the E221K variant. In addition, a boronic acid transition state inhibitor, LP-06, lowered the ceftolozane and ceftazidime MICs by 8-fold for the E221K-expressing strain. Understanding these structural changes in evolutionarily selected variants is critical toward designing effective β-lactam/β-lactamase inhibitor therapies for *P. aeruginosa* infections.

IMPORTANCE The presence of β-lactamases (e.g., PDC-3) that have naturally evolved and acquired the ability to break down β-lactam antibiotics (e.g., ceftazidime and ceftolozane) leads to highly resistant and potentially lethal *Pseudomonas*

Received 19 September 2018 **Accepted** 16 October 2018 **Published** 11 December 2018

Citation Barnes MD, Taracila MA, Rutter JD, Bethel CR, Galdadas I, Hujer AM, Caselli E, Prati F, Dekker JP, Papp-Wallace KM, Haider S, Bonomo RA. 2018. Deciphering the evolution of cephalosporin resistance to ceftolozane-tazobactam in *Pseudomonas aeruginosa*. mBio 9:e02085-18. https://doi.org/10.1128/mBio.02085-18.

Editor George A. Jacoby, Lahey Hospital and Medical Center

Address correspondence to Robert A. Bonomo, robert.bonomo@va.gov.

M.D.B. and M.A.T. contributed equally to the manuscript.

aeruginosa infections. We show that wild-type PDC-3 β-lactamase forms an acyl enzyme complex with ceftazidime, but it cannot accommodate the structurally similar ceftolozane that has a longer R2 side chain with increased basicity. A single amino acid substitution from a glutamate to a lysine at position 221 in PDC-3 (E221K) causes the tyrosine residue at 223 to adopt a new position poised for efficient hydrolysis of both cephalosporins. The importance of the mechanism of action of the E221K variant, in particular, is underscored by its evolutionary recurrences in multiple bacterial species. Understanding the biochemical and molecular basis for resistance is key to designing effective therapies and developing new β-lactam/β-lactamase inhibitor combinations.

KEYWORDS AmpC, PDC-3, antibiotic resistance, beta-lactam, beta-lactamase, ceftolozane, omega loop

Pseudomonas aeruginosa infections are among the most serious health threats of this century, mostly hospital acquired by immunocompromised patients. *P. aeruginosa* is responsible for approximately 51,000 nosocomial infections every year in the United States (1), and it is one of the top three pathogens of global concern specifically addressed by the World Health Organization in their guidelines for prevention and control released late in 2017 (2). In a survey that identified more than 400,000 drug-resistant pathogens collected from 4,515 U.S. hospitals between 2011 and 2014, *P. aeruginosa* was the 6th most common nosocomial pathogen, ranking 2nd in ventilator-associated pneumonia and 3rd in catheter-associated urinary tract infections (3). Particularly notorious in cystic fibrosis, *P. aeruginosa* infects 80% of patients by 18 years of age and results in a 2.6-fold increase in mortality. Alarming levels of resistance are emerging without compensatory therapies to overcome these infections. *P. aeruginosa* produces a chromosomally encoded class C cephalosporinase (*Pseudomonas*-derived cephalosporinase, PDC β-lactamase) that is often responsible for high-level resistance to β-lactam antibiotics.

Ceftolozane, a "fifth-generation" cephalosporin, is characterized by a 3′ aminopyrazolium substitution in the R2 side chain (Fig. 1) and is commercially partnered with tazobactam, a penicillin sulfone and irreversible β-lactamase inhibitor. The ceftolozane-tazobactam combination is active against *P. aeruginosa* isolates resistant to ceftazidime, carbapenems, and piperacillin-tazobactam. The advantage of the ceftolozane-tazobactam combination is that ceftolozane is more stable to PDC hydrolysis than the predecessor β-lactam partner of tazobactam (i.e., piperacillin). Importantly, PDCs are not efficient at hydrolyzing ceftolozane (4). Unlike tazobactam, ceftolozane inhibits penicillin binding proteins (PBPs), allowing tazobactam to target other serine β-lactamases (e.g., TEM-1) and ESBLs (e.g., CTX-M-15) that are often present in *P. aeruginosa*. Alarmingly, resistance to new antibiotics is often reported before FDA approval (5). Indeed, resistance to ceftolozane-tazobactam has already emerged and may prove to be a significant clinical threat (6–8).

Among the resistance mechanisms is the evolution of the PDC β-lactamase amino acid variants that often increase catalysis and spectrum of cephalosporin hydrolysis. Conserved motifs within the AmpC β-lactamases, largely the Ω-loop and H10 helix of the R2 region, seem particularly prone to amino acid substitutions (Fig. 2), insertions, and deletions that enlarge the active site and accommodate bulkier R1 and R2 groups of the β-lactam, respectively (9, 10). Several PDC Ω-loop variants (PDC-50 V213A; PDC-74, -75, and -78 G216R; PDC-79 and -86 E221K; PDC-80 E221G; and PDC-85 Y223H) identified originally in highly drug-resistant *P. aeruginosa* clinical isolates conferred resistance to a panel of antibiotics, including ceftazidime and ceftolozane-tazobactam (11, 12). Herein, we assessed the contribution of these residues (V213, G216, E221, and Y223) in PDC-3 toward ceftolozane-tazobactam and ceftazidime resistance by performing a structure-function analysis. In addition, the E221K variant was selected for in-depth biochemical analysis, revealing robust hydrolysis of ceftolozane as well as ceftazidime. Importantly, we find that avibactam restored in the strains expressing the variants susceptibility to ceftolozane and ceftazidime. The boronic acid transition state

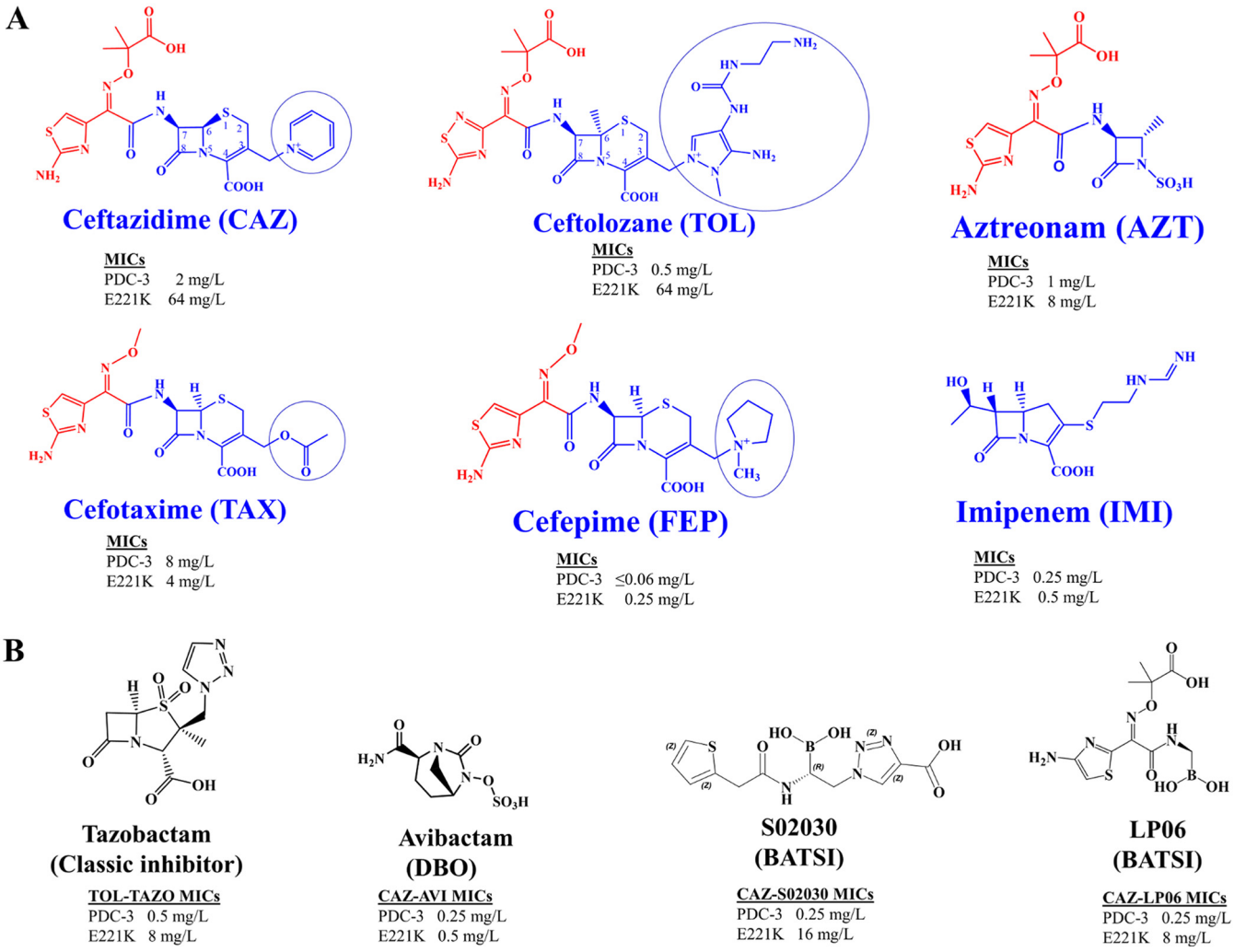

FIG 1 Structures of β-lactam antibiotics (A) and inhibitors (B) tested in the MIC assays. The R1 side chains of the β-lactam antibiotics are shown in red, and the R2 side chains of the cephalosporins are circled. MIC values from Table 1 are listed for PDC-3 versus E221K.

inhibitors (BATSIs) also lowered ceftolozane and ceftazidime MICs of strains harboring the variants, but the E221K strain maintained modestly high MICs (8 to 16 mg/liter). Our analysis presented herein provides the first biochemical and molecular dynamics rationale for enhanced catalytic action against this novel 3′ aminopyrazolium cephem.

RESULTS AND DISCUSSION

Single amino acid substitutions in the Ω-loop of PDC-3 enhance resistance toward ceftolozane and ceftazidime. Previously, five different amino acid substitutions in the Ω-loop (V213A, G216R, E221K, E221G, and Y223H) of the PDC β-lactamase were found to confer enhanced β-lactam resistance in clinical isolates (12). Consistent with this finding, a 5-amino-acid-residue deletion, which included E221 and Y223, and a 7-amino-acid-residue deletion, including V213 and G216, in PDC β-lactamases was concomitant with increased resistance to ceftazidime-avibactam (13). In response to selective pressure using ceftolozane-tazobactam, the evolution of the E221K (E247K including the signal peptide sequence) emerged in a *Pseudomonas* strain (11). This particular amino acid substitution arose in SRT-1 of *Serratia marcescens* as early as 20 years ago (9, 14). To study the role of each of these residues in the mechanism of resistance and anticipate therapeutic approaches against the variants, we engineered the V213A, V213G, G216A, G216R, E221A, E221K, E221G, Y223A, and Y223H variants in

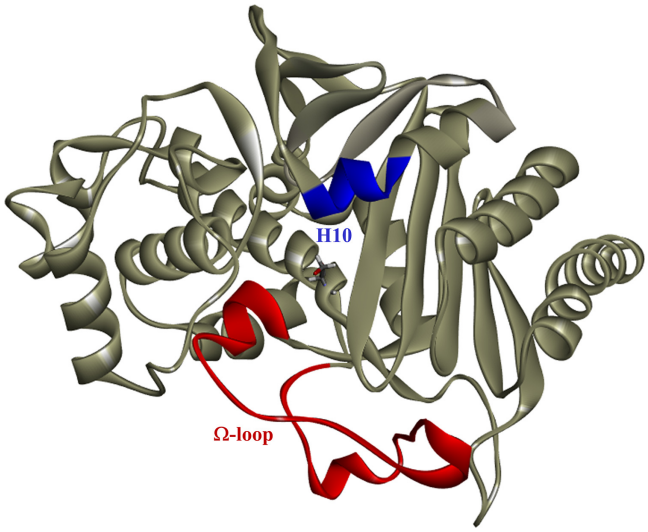

FIG 2 PDC structure (PDB ID 4HEF) showing the Ω-loop (red) at the entrance of the active site and the H10 helix (blue) of the R2 region that accommodates the R2 side chain of cephalosporins. The active site serine is shown in stick model representation.

PDC-3 for susceptibility determinations, followed by a focused analysis of the E221K variant's interactions with ceftolozane and ceftazidime.

The susceptibility of the variants expressed in an isogenic *Escherichia coli* DH10B background was tested against a panel of representative cephalosporins, penicillins, monobactams, and carbapenems (Table 1). Amino acid substitutions in PDC-3 led to the most significant impact on MICs against ceftolozane, ceftazidime, and aztreonam. Interestingly, the structures of ceftolozane, ceftazidime, and aztreonam contain the "bulkiest" and most hydrophilic R1 groups of the compounds tested (Fig. 1A). The dimethylacetic acid in the R1 group in ceftazidime (also found in ceftolozane and aztreonam) was specifically associated with antipseudomonal activity (15). The E221K variant conferred the greatest resistance with an increase of 128-fold in the ceftolozane MIC and an increase of 32-fold in ceftazidime MIC relative to that of the wild-type strain (Table 1).

TABLE 1 Susceptibility results of various β-lactams against PDC-3 and the variants expressed in the pBC SK (-) vector in *E. coli* DH10B cells

Species and strain[a]	MIC value (mg/liter)							
	Ceftolozane	Ceftazidime	Cefotaxime	Cefepime	Ampicillin	Piperacillin	Aztreonam	Imipenem
P. aeruginosa								
18SH	8	64	>256	128	4,096	512	128	2
PAO1	0.5	1	16	4	2,048	4	4	2
E. coli								
DH10B	0.5	0.25	<0.06	0.125	4	2	0.125	0.5
DH10B pBC SK	0.5	0.25	<0.06	<0.06	4	2	0.125	0.25
DH10B pBC SK bla_{PDC-1}	0.5	2	8	0.125	256	16	0.5	0.25
DH10B pBC SK bla_{PDC-3}	0.5	2	8	0.06	256	16	1	0.25
DH10B pBC SK $bla_{PDC-3\ V213A}$	4	32	16	0.125	1,024	64	8	0.5
DH10B pBC SK $bla_{PDC-3\ V213G}$	4	16	16	0.125	1,024	64	8	0.5
DH10B pBC SK $bla_{PDC-3\ G216R}$	8	32	16	0.25	1,024	16	16	0.5
DH10B pBC SK $bla_{PDC-3\ G216A}$	2	16	8	0.125	1,024	64	8	0.5
DH10B pBC SK $bla_{PDC-3\ E221K}$	64	64	4	0.25	256	16	8	0.5
DH10B pBC SK $bla_{PDC-3\ E221G}$	16	32	8	0.125	512	64	4	0.5
DH10B pBC SK $bla_{PDC-3\ E221A}$	2	8	16	0.125	1,024	128	4	0.5
DH10B pBC SK $bla_{PDC-3\ Y223H}$	8	16	8	0.125	512	32	4	0.5
DH10B pBC SK $bla_{PDC-3\ Y223A}$	32	32	16	0.25	256	16	4	0.5

[a]*P. aeruginosa* 18SH and *P. aeruginosa* PAO1 are control strains expressing PDC-3 and PDC-1, respectively.

TABLE 2 Susceptibility results of various β-lactams compared to β-lactams in combination with β-lactamase inhibitors against PDC-3 and variants expressed in the pBC SK (-) vector in *E. coli* DH10B cells

Species and strain[a]	MIC value (mg/liter)[b]										
	PIP	PIP-TAZ	TOL	TOL-TAZ	TOL-AVI	TOL-LP06	TOL-S02030	CAZ	CAZ-AVI	CAZ-LP06	CAZ-S02030
P. aeruginosa											
18SH	512	256	8	8	8	8	8	64	2	32	64
PAO1	4	4	0.5	0.5	0.5	0.5	0.5	1	1	0.5	1
E. coli											
DH10B	2	2	0.5	0.25	0.5	0.5	0.25	0.25	0.25	≤0.25	0.25
DH10B pBC SK	2	2	0.5	0.25	0.25	0.25	0.25	0.25	0.25	≤0.25	0.25
DH10B pBC SK bla_{PDC-1}	16	8	0.5	0.5	0.5	0.25	0.25	2	0.25	0.25	0.25
DH10B pBC SK bla_{PDC-3}	16	4	0.5	0.5	0.5	0.25	0.25	2	0.25	0.25	0.25
DH10B pBC SK $bla_{PDC-3\ V213A}$	64	16	4	2	0.5	0.25	0.25	32	0.25	0.25	1
DH10B pBC SK $bla_{PDC-3\ V213G}$	64	8	4	2	0.5	0.25	0.25	16	0.25	0.25	1
DH10B pBC SK $bla_{PDC-3\ G216R}$	16	8	8	4	0.25	0.5	0.5	32	0.25	0.25	1
DH10B pBC SK $bla_{PDC-3\ G216}$	64	8	2	2	0.25	0.25	0.25	16	0.25	0.25	0.25
DH10B pBC SK $bla_{PDC-3\ E221K}$	16	8	64	8	1	8	8	64	0.5	8	16
DH10B pBC SK $bla_{PDC-3\ E221G}$	64	16	16	4	0.5	1	2	32	0.5	0.5	1
DH10B pBC SK $bla_{PDC-3\ E221}$	128	16	2	2	0.5	0.5	0.25	8	0.25	0.25	0.25
DH10B pBC SK $bla_{PDC-3\ Y223H}$	32	4	8	1	0.25	0.5	0.5	16	0.5	0.5	2
DH10B pBC SK $bla_{PDC-3\ Y223A}$	32	4	32	4	1	2	8	32	0.5	0.5	8

[a]*P. aeruginosa* 18SH and *P. aeruginosa* PAO1 are control strains expressing PDC-3 and PDC-1, respectively.
[b]PIP, piperacillin; TAZ, tazobactam; TOL, ceftolozane; AVI, avibactam; CAZ, ceftazidime.

Avibactam and boronic acid transition state inhibitors (BATSIs) overcome resistance to ceftazidime. Several β-lactam–β-lactamase inhibitor combinations were selected to test the efficacy of compounds from three different classes of inhibitors against the strains expressing the variant PDCs. Susceptibility was tested against tazobactam, a first-generation sulfone inhibitor, combined with piperacillin or ceftolozane; avibactam (16), a diazabicyclooctane (DBO) combined with ceftazidime; and two boronic acid transition state inhibitors (BATSIs) (a cephalothin analog S02030 [17] and a ceftazidime analog LP-06 [18]) (see Fig. 1B for structures), each combined with ceftazidime.

In the piperacillin-tazobactam and ceftolozane-tazobactam combinations, tazobactam led to a 2- to 8-fold attenuation of the variant strain MICs compared to those of the single antibiotic (Table 2). The E221K variant conferred the greatest resistance to ceftolozane and ceftazidime. Susceptibility to ceftolozane and ceftazidime was substantially restored when these oxyimino cephalosporins were paired with avibactam (MICs ≤ 1 mg/liter). In other studies, select Ω loop variants were associated with resistance to these clinically available combination therapies (12, 13). Therefore, we extended the study to include testing of BATSI inhibitors, which are chemically distinct from tazobactam and avibactam (Fig. 1). Interestingly, the LP-06 and S02030 BATSIs lowered the MIC values of ceftolozane and ceftazidime for all variant strains, but the strain expressing E221K maintained the highest MICs (8 to 16 mg/liter) (Table 2). LP-06 lowered the MICs more effectively than S02030 did, particularly for the Y223A variant strain. Further, LP-06 was as potent as avibactam in all variant strains except the strain harboring the E221K variant.

Protein expression of PDC-3 and the E221K variant in the cell is lower than the other variants. To determine whether the elevated MIC values for the E221K variant strain were due to a higher expression level of the β-lactamase protein in the cell, we developed and used an anti-PDC-3 antibody to perform immunoblotting on the strains harboring PDC-3 and the variants (Fig. 3). *E. coli* strains variably expressed each PDC-3 variant. On the basis of the epitope mapping of PDC-3 using a SPOT-synthesis technique, we posit that changes in the binding of the anti-PDC-3 antibody to the newly introduced amino acids in the variants does not account for differences in intensities in the immunoblot; the epitopes do not encompass the V213, G216, E221, and Y223 amino acid residues (Fig. S1). Strikingly, the amount of the E221K variant most closely

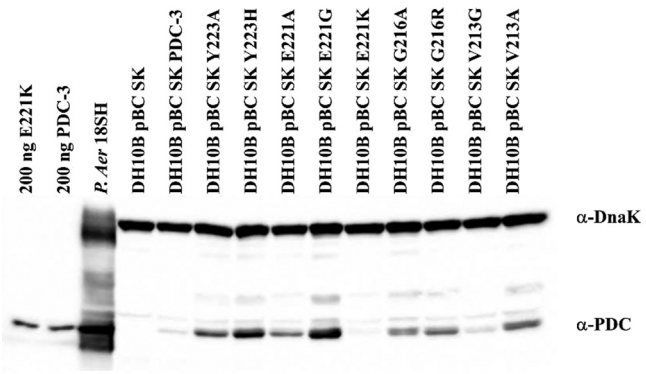

FIG 3 Immunoblots of *E. coli* DH10B whole-cell lysates of PDC-3 and variants expressed in the pBC SK (-) vector. The *P. aeruginosa* 18SH clinical isolate and purified PDC-3 β-lactamase are used as positive controls. An anti-DnaK antibody was used as a loading control.

mimicked the low expression of wild-type PDC-3 β-lactamase. Further, the E221K variant was detected at the lowest level of expression relative to the other variants, a remarkable observation when considering that the E221K variant confers the highest level of resistance against the tested antibiotics (Tables 1 and 2). Supporting this observation, previous studies suggested that overexpression of PDC proteins alone is not always sufficient to account for such robust resistance (11, 12, 19). To further explore the mechanisms of resistance, we tested the β-lactam kinetic characteristics of the E221K variant.

Mechanisms of catalysis: PDC-3 β-lactamase fails to establish an acyl complex with ceftolozane but forms a prolonged acyl-complex with ceftazidime. The wild-type PDC-3 hydrolyzed ceftolozane and ceftazidime albeit poorly (Fig. 4A and B), consistent with the MIC results. As expected, PDC-3 demonstrated a lower K_m toward ceftazidime compared to ceftolozane. Using a competitive inhibition assay with nitrocefin as the reporter substrate, the $K_{i\ app}$ of ceftolozane (1.3 mM) was determined to be 60-fold higher than that of ceftazidime (22 μM) with PDC-3. Thus, PDC-3 interacts favorably with ceftazidime compared to ceftolozane, yet is not hydrolyzed (Fig. 4B).

To further investigate the catalytic mechanism, we performed timed mass spectrometry. Two isoforms of PDC-3 and E221K were expressed and purified due to the presence of additional methionine at the N terminus (20) (Fig. 5). Using a 1:1 molar ratio of enzyme to substrate, timed mass spectrometry analysis captured the binding of PDC-3 to ceftazidime, but not to ceftolozane (Fig. 5 and Table 3). The observed masses reflect cephalosporins without the R2 group (circled in Fig. 2). Cephalosporins that demonstrate efficient R2 elimination typically have more reactive β-lactam rings and enhanced activity (21). Elimination of the R2 group from cephalosporins results from electron transfer upon binding to β-lactamases and was previously shown for ceftazidime and ceftolozane among other cephalosporins (21–25). An acyl-complex with ceftolozane or ceftazidime was not detected with the E221K variant, but ceftazidime without its R2 group was captured in complex with PDC-3 (Fig. 5).

As indicated by a lower K_m, nearly 60-fold-lower apparent inhibition constant (1.3 mM ceftolozane $K_{i\ app}$ versus 22 μM ceftazidime $K_{i\ app}$), and the ability to capture the ceftazidime acylated PDC-3 complex, ceftazidime must be able to occupy the active site of PDC-3 despite overall hydrolytic deficiency. Contrary to ceftazidime, the failure of PDC-3 to hydrolyze ceftolozane is more likely due to the inability of the PDC-3 active site to accommodate the more basic and extended 3′ aminopyrazolium-containing R2 side chain of ceftolozane (Fig. 2) and form an acyl-complex (see "Molecular modeling" below). We also have not ruled out product inhibition as a mechanism. Modifications of the 3-aminopyrazolium side chains during the structural derivation of ceftolozane correlated with stability to class C β-lactamases, likely due to steric hindrance (26). The mechanisms of these third-generation cephalosporins contrast with that of the fourth-

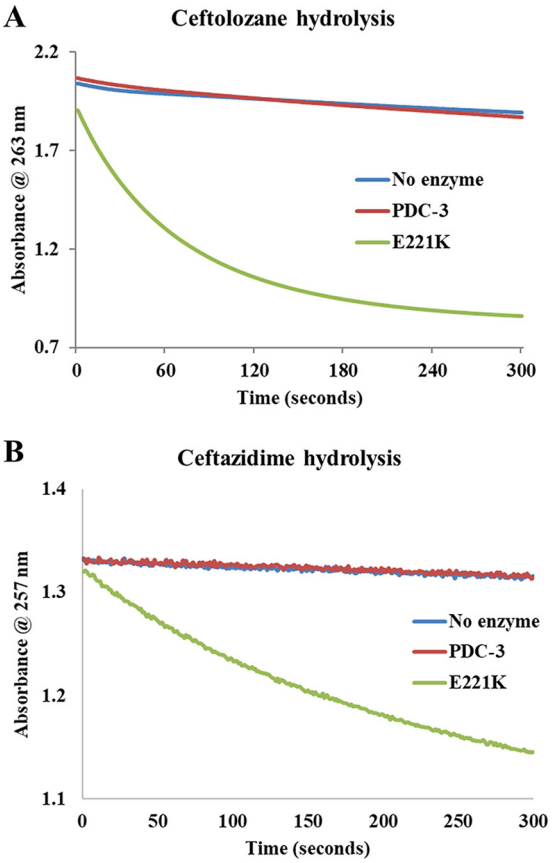

FIG 4 Hydrolysis of ceftolozane (A) and ceftazidime (B) by PDC-3 and the E221K variant. Ceftolozane (100 μM) was tested with 1 μM enzyme (PDC-3 or E221K). Ceftazidime (300 μM) was assayed with 100 nM enzyme (PDC-3 or E221K).

generation cephalosporin cefepime, which has a zwitterionic quaternary amine as the R2 group that decreases affinity for β-lactamases (Fig. 1) (27) and effectively overcomes resistance conferred by the PDC variants in *E. coli* (Table 1).

Acquisition of hydrolytic efficiency: the E221K variant demonstrates robust hydrolysis of ceftolozane and ceftazidime. Consistent with increased resistance of the variants compared to PDC-3 (Table 1 and 2), the E221K variant acquired an ability to efficiently hydrolyze ceftolozane (Fig. 4A) and ceftazidime (Fig. 4B). K_m for the E221K variant for ceftazidime is 174 $\pm$ 20 μM (Table 4), considerably higher than previously reported values of 35 μM (28) and 51.7 $\pm$ 2.1 μM (20) for PDC-3. Turnover (k_{cat}) for E221K for ceftazidime is 9 $\pm$ 1 s^{-1} (Table 5), substantially greater than the 0.02 s^{-1} (28) and 0.002 s^{-1} (4) values reported for PDC-3. Catalytic efficiency (k_{cat}/K_m) for E221K (5.2 $\pm$ 0.8 $\times$ 10^{-2} μM^{-1} s^{-1}) is notably higher for ceftazidime than the reported values of PDC-3; 0.0006 μM^{-1} s^{-1} (28) and 0.00033 μM^{-1} s^{-1} (4).

E221K exhibited a higher K_m value for ceftolozane (341 $\pm$ 64 μM) than for ceftazidime (174 $\pm$ 20 μM) (Table 4). The other kinetic parameters were similar for E221K between the substrates: ceftolozane (k_{cat} of 10 $\pm$ 1 s^{-1} and k_{cat}/K_m of 0.029 $\pm$ 0.006 μM^{-1} s^{-1}) and ceftazidime (k_{cat} of 9 $\pm$ 1 s^{-1} and k_{cat}/K_m of 0.052 $\pm$ 0.008 μM^{-1} s^{-1}) (Table 4). The efficient hydrolysis of ceftolozane and ceftazidime by E221K is consistent with the inability to capture the acyl-E221K complexes by timed mass spectrometry due to the rapidity of the reaction (Fig. 5).

The BATSIs are potent inhibitors of PDC-3 and the E221K variant. The steady-state inhibitory kinetics of the BATSIs were assessed using nitrocefin as a reporter substrate (nitrocefin K_m for PDC-3 (20 $\pm$ 2 μM) and E221K (17 $\pm$ 3 μM)). S02030, the cephalothin analog, and LP-06, the ceftazidime analog, inhibit PDC-3 and the E221K

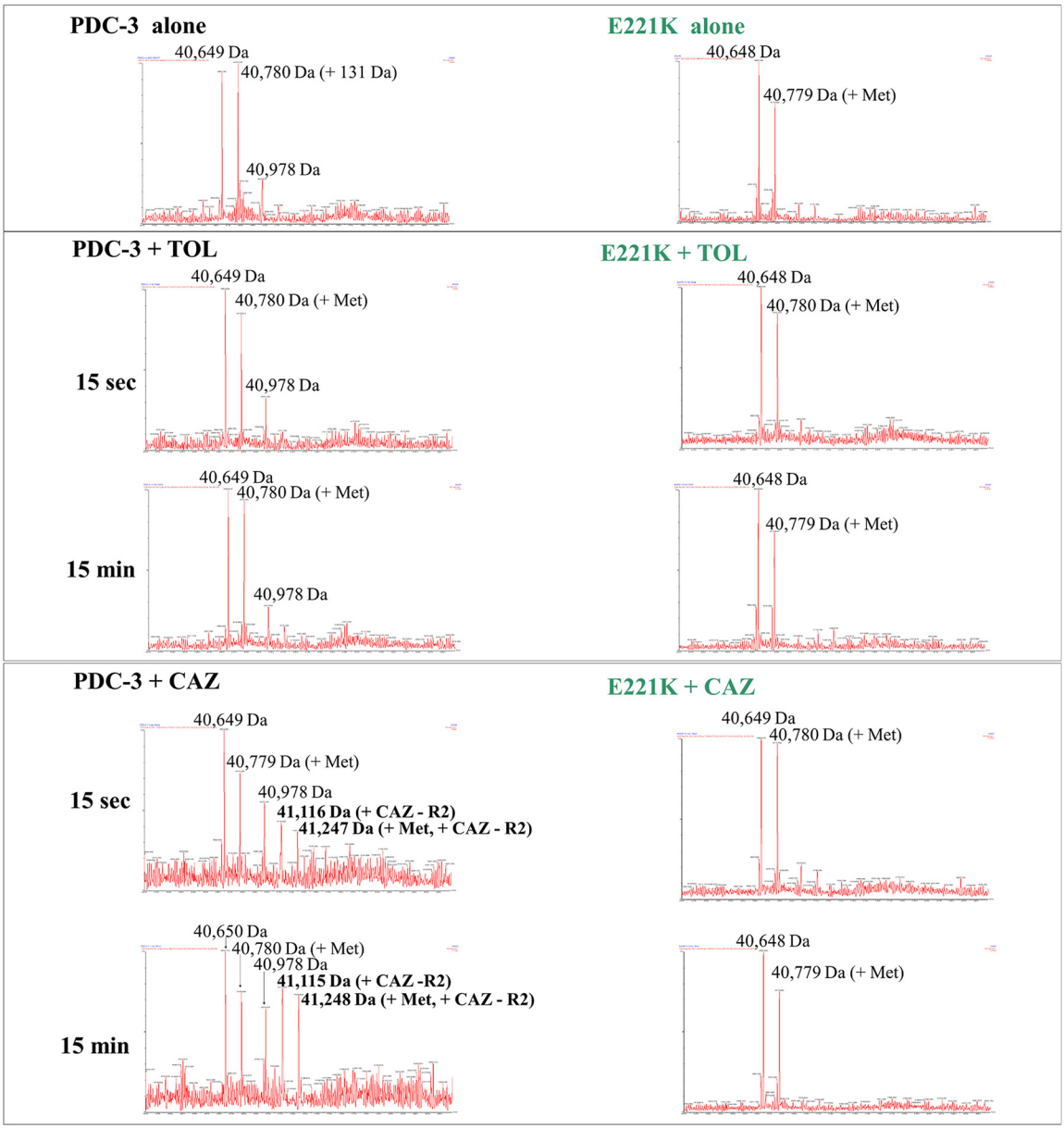

FIG 5 Electrospray ionization mass spectrometry (ESI-MS) of pure PDC-3 and the E221K variant incubated with ceftolozane (TOL) (MW, 666 Da; MW without R2 group, 471 Da) or ceftazidime (CAZ) (MW without R2 group, 468 Da) for 15 s or 15 min at a 1:1 molar ratio. Methionine (Met) has a molecular weight of 131 Da. Mass accuracy is ±5 Da.

variant at nanomolar concentrations. LP-06 and S02030 inhibited PDC-3 more efficiently than E221K did (Table 5). Comparison between the two inhibitors suggests that LP-06 has superior inhibitory activity compared to S02030 for both PDC-3 and E221K (Table 5).

BATSI inhibitors increase the thermodynamic stability of PDC-3 and E221K. The thermodynamic stability of PDC-3 and E221K was determined from equilibrium unfolding curves (Fig. 6). Thermal denaturation revealed that the E221K variant is less stable compared to PDC-3 (T_m of 45°C and 52°C, respectively), with a $\Delta\Delta Gu = 2.32 \pm 0.2$ Kcal/mol loss in stability (Fig. 6). Binding of the S02030 BATSI inhibitor to either PDC-3 or the E221K variant increased the stability (6°C increase for PDC-3 and 3 to 4°C increase for the variant) (Fig. 6A). Similarly, the LP-06 BATSI stabilized both PDC-3 (6°C increase) and E221K (5°C increase) (Fig. 6B), as previously observed for other BATSIs with SHV-1, ADC-7, and AmpC (29–32). Increased stability between the inhibitors and the

TABLE 3 Predicted masses of PDC-3 and the E221K variant β-lactamases with and without the addition of ceftazidime and ceftolozane[a]

Predicted Masses (Da) of β-lactamases and adducts (± 5 Da)			
Change in structure	Change in mass	PDC-3	E221K
		40,648	40,648
+Methionine (Met)	+ 131	40,779	40,779
+CAZ (no R2 group) 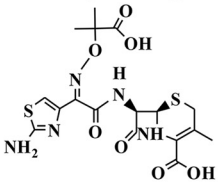	+ 468	41,116	41,116 Not detected
+Methionine (Met) +CAZ (no R2 group) 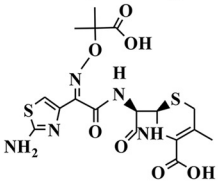	+599	41,247	41,247 Not detected
+TOL (no R2 group) 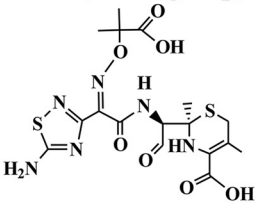	+471	41,119 Not detected	41,119 Not detected
+Methionine (Met) +TOL (no R2 group) 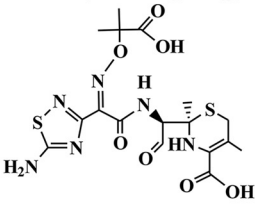	+602	41,250 Not detected	41,250 Not detected

[a]Predicted masses of PDC-3 and the E221K variant β-lactamases with and without the addition of ceftazidime (CAZ) and ceftolozane (TOL). The R2 group is eliminated from the cephalosporin upon binding to β-lactamase. The additional Met residue was a result of cloning and does not impact β-lactamase activity.

β-lactamases is indicative of higher energy for noncovalent interaction in the covalent acyl complexes compared to the β-lactamase alone (31). Thus, increased stability of PDC-3 with the BATSIs, reflective of increased interactions and the formation of inhibitory complexes, would predict the lower ceftazidime-BATSI MICs compared to ceftazidime alone MICs in Table 2.

Notably, the thermal denaturation profiles showed a further distinction between PDC-3 and the E221K variant. The transition where the inhibitor-bound PDC-3 began to

TABLE 4 Steady-state kinetics of the E221K variant with ceftazidime and ceftolozane[a]

Parameter	E221K-ceftolozane	E221K-ceftazidime
V_{max} (μM/s)	1.0 ± 0.1	0.9 ± 0.1
K_m (μM)	341 ± 64	174 ± 20
k_{cat} (s^{-1})	10 ± 1	9 ± 1
k_{cat}/K_m (μM^{-1} s^{-1})	(2.9 ± 0.6) × 10^{-2}	(5.2 ± 0.8) × 10^{-2}

[a]PDC-3 hydrolysis of ceftolozane and ceftazidime was negligible.

unfold occurred at 4°C, higher than for PDC-3 alone, shifting the curve for the inhibitor-bound PDC-3 to the right (Fig. 6). After the initial transition, PDC-3 unfolded at a similar rate with and without inhibitor as reflected by a uniform difference (~4°C) between the two melting curves (Fig. 6). Conversely, the E221K variant started to unfold at the same temperature regardless of whether it was bound by inhibitor, but the steeper slope of E221K alone suggested a higher rate of unfolding in the absence of inhibitor.

The lower unfolding rate of inhibitor-bound E221K compared to inhibitor-bound PDC-3 could be due to additional interactions between the LP-06 and E221K as suggested by our molecular modeling (Fig. 7). The boronic and carboxylic acids of LP-06 interact with residue S319 in PDC-3. In the E221K variant, the interaction between the boronic acid and S319 is maintained, but the carboxylic acid-S319 bond is lost. Further, LP-06 forms new bonds with the S319, N320, Q120, and Y151 residues of E221K. To further explore the structural changes in the E221K compared to PDC-3, we employed molecular modeling and molecular dynamic simulations using ceftolozane as the substrate.

Molecular dynamic simulations reveal conformational changes in the E221K variant that accommodate binding of ceftolozane. Classical atomistic molecular dynamics (MD) and well-tempered metadynamics simulations (WT-MetaD) were carried out to enhance conformational sampling of PDC-3 and variants (Fig. 8). Free energy surface (FES) plots were calculated for each system, highlighting basins of lowest energy states as shown in the red wells in Fig. 8 (e.g., e1 and k1), wherein each basin corresponds to an ensemble of conformations of the protein. Conformations of PDC-3 and the variants were extracted from the free energy minima and superimposed onto the crystal structure (PDB ID, 4HEF, yellow).

The E221K variant adopts conformations in the free-energy landscape that are not accessible by PDC-3 (E221) (Fig. 8). Generally, the E221 variants are able to explore the conformation in k1, a1, and g1 energy basins that are similar to the conformation in the wild-type (e1) (Fig. 8B to D). However, other energy basins such as k3 are observed exclusively by the E221K variant (Fig. 8B). Moreover, the clustered (representative) structures illustrate that the conformation adopted by the Ω-loop in particular is distinct from that of the crystal structure. Consistent with the conformational changes, the hydrogen bonding patterns are altered in the E221 variants. In PDC-3, the side chain of E221 forms hydrogen bonds with K67, but these bonds are disrupted in the E221K, E221A, and E221G variants.

In the Michaelis-Menten complex, rotation of the Y223 residue in E221K supports binding of ceftolozane. Enhanced sampling simulations identified conformations in the E221K variant, which were not found in the wild type. The conformations

TABLE 5 Inhibition kinetics of PDC-3 and the E221K variant with the BATSI compounds[a]

	IC_{50} (nM) for β-lactamase with:	
β-Lactamase (IC_{50})	LP-06	S02030
PDC-3 (1.5 nM)	9 ± 1	62 ± 2
E221K (20 nM)	342 ± 20	769 ± 30

[a]Inhibition kinetics of PDC-3 and the E221K variant with the BATSI compound LP-06 or S02030, determined after a 5-min preincubation with LP-06 or S02030 with cell lysate. Nitrocefin was used as the reporter substrate.

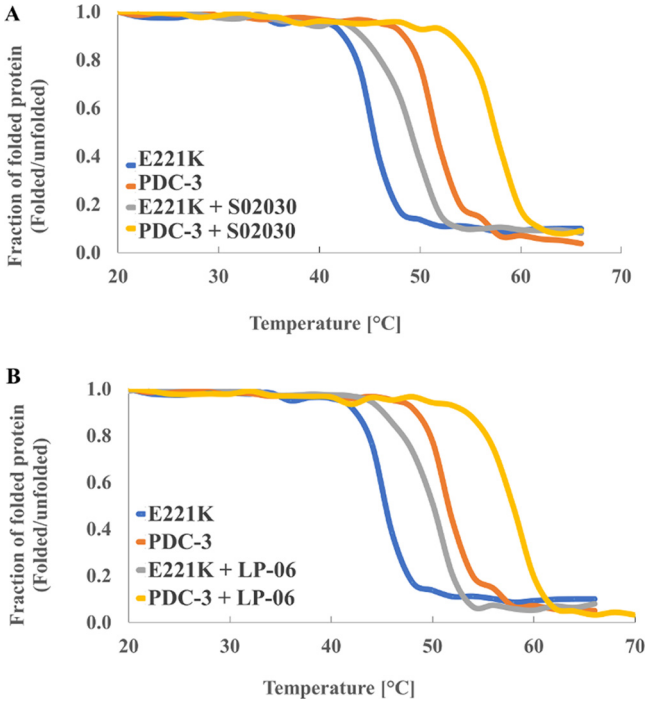

FIG 6 Thermal denaturation of PDC-3 and E221K with S02030 (A) or LP-06 BATSI (B) inhibitors, expressed as a ratio of folded protein to unfolded protein.

identified for E221K indicated a rotation of the Y223 side chain. The Y223 residue in PDC-3 adopts several positions within the same plane (Fig. 9A), whereas in the E221K variant, Y223 flips into a perpendicular plane, opening a hidden cavity adjacent to the catalytic site (Fig. 9B), which is occluded by Y223 in the crystalline form of PDC-3. These data are supported by previous work in *E. coli* class C cephalosporinases, where a steric clash between the tyrosine ring and R1 cephalosporin side chains was concluded from the crystal structure of AmpC with a glycine substitution in the Y223-equivalent residue (Y221G) of PDC (33). Increased flexibility in the Ω-loop was also observed in the crystal structure of the E221K analog of AmpC of *E. coli* (E219K) (33). This newly adopted conformation and change in the architecture of the Ω-loop facilitate the formation of Michaelis-Menten complex between the E221K variant and ceftolozane. The aminopyrazole group in the R2 side chain of ceftolozane seems to be the specific moiety responsible for its inability to bind to PDC-3. These data are supported by measurable steady-state kinetic parameters (e.g., K_m of 341 ± 64 μM) (Table 4) and elevated MICs (ceftolozane MIC PDC-3 of 0.5 μM → E221K 64 μM) (Table 2).

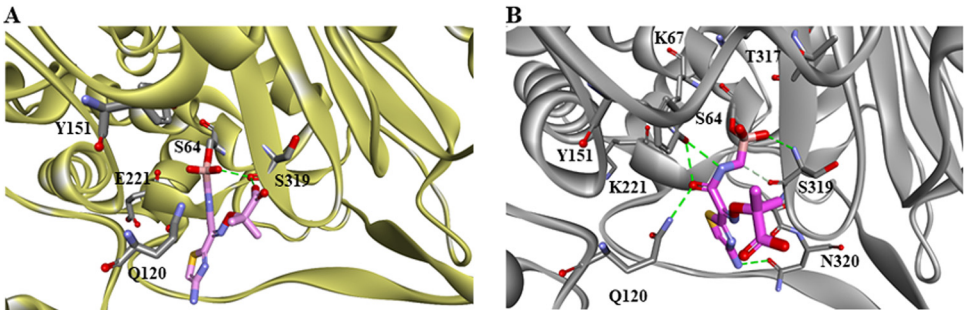

FIG 7 Molecular modeling of PDC-3 (A) and the E221K variant (B) bound to LP-06, a ceftazidime-like BATSI. LP-06 is represented as a stick figure with carbon in pink, sulfur in yellow, nitrogen in purple, oxygen in red, and boron in rose color.

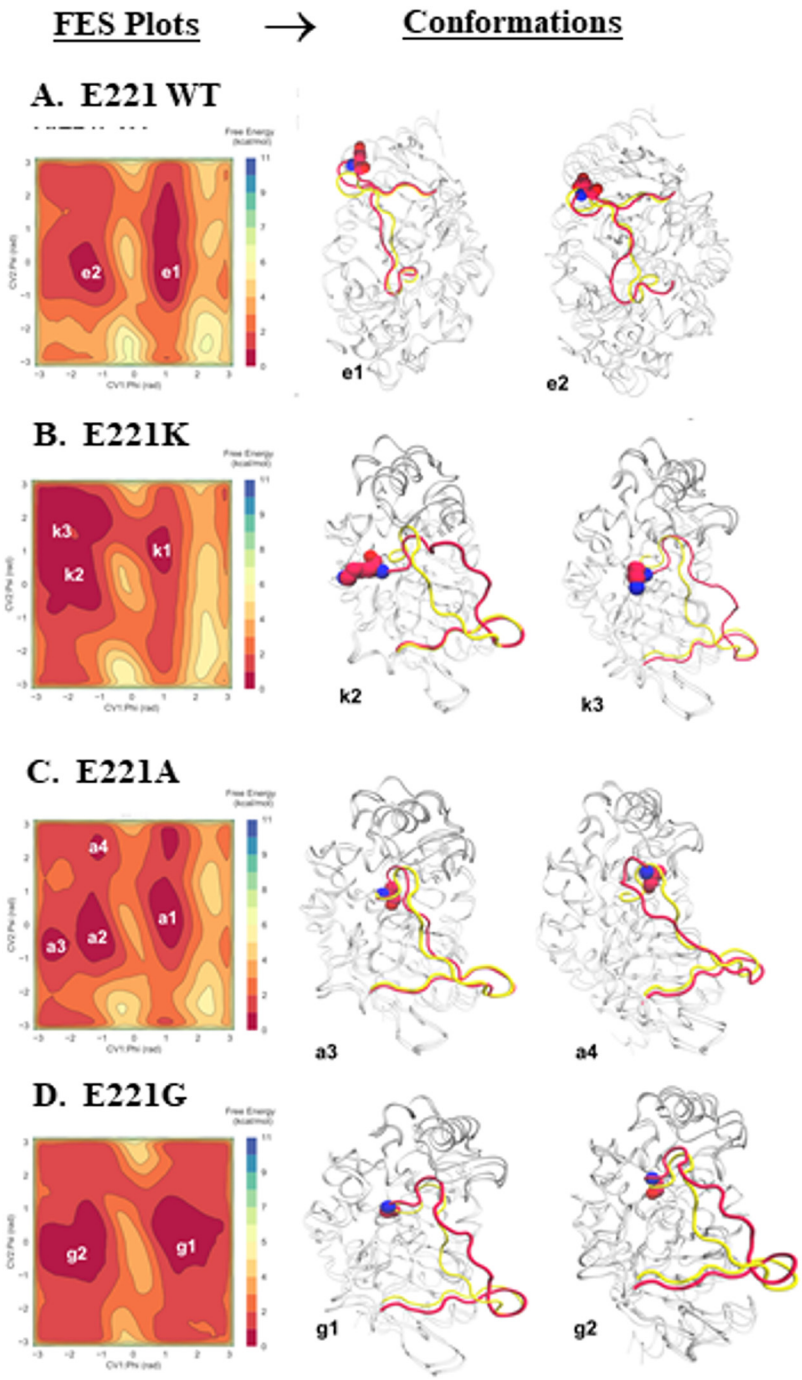

FIG 8 Conformational free energy surface (FES) reconstructed from metadynamics simulations of PDC-3 (A) and the E221 variants E221A (B), E221K (C), and E221G (D). Representative conformations corresponding to each energy basin (e.g., e1, e2) are superimposed onto the crystal structure, shown on the right. The Ω-loop of the crystal structure of wild-type E221 (yellow) and the simulated result of the structure (red) are highlighted. The amino acid of interest (wild-type E221 or the A, K, and G substitutions) in each panel is visualized in red and blue using a Corey-Pauling-Koltun (CPK) representation.

In the acyl-complex, ceftolozane interacts favorably with the E221K variant, but it is unable to interact productively with PDC-3. Connolly representations depict overt changes in electrostatic potential when the E221 residue is changed to a lysine (Fig. 9C and D). Y223 and E221 are located in the center of the green circle in Fig. 9C and D. The calculated potential of PDC-3 is 1318 kT compared to the potential of the

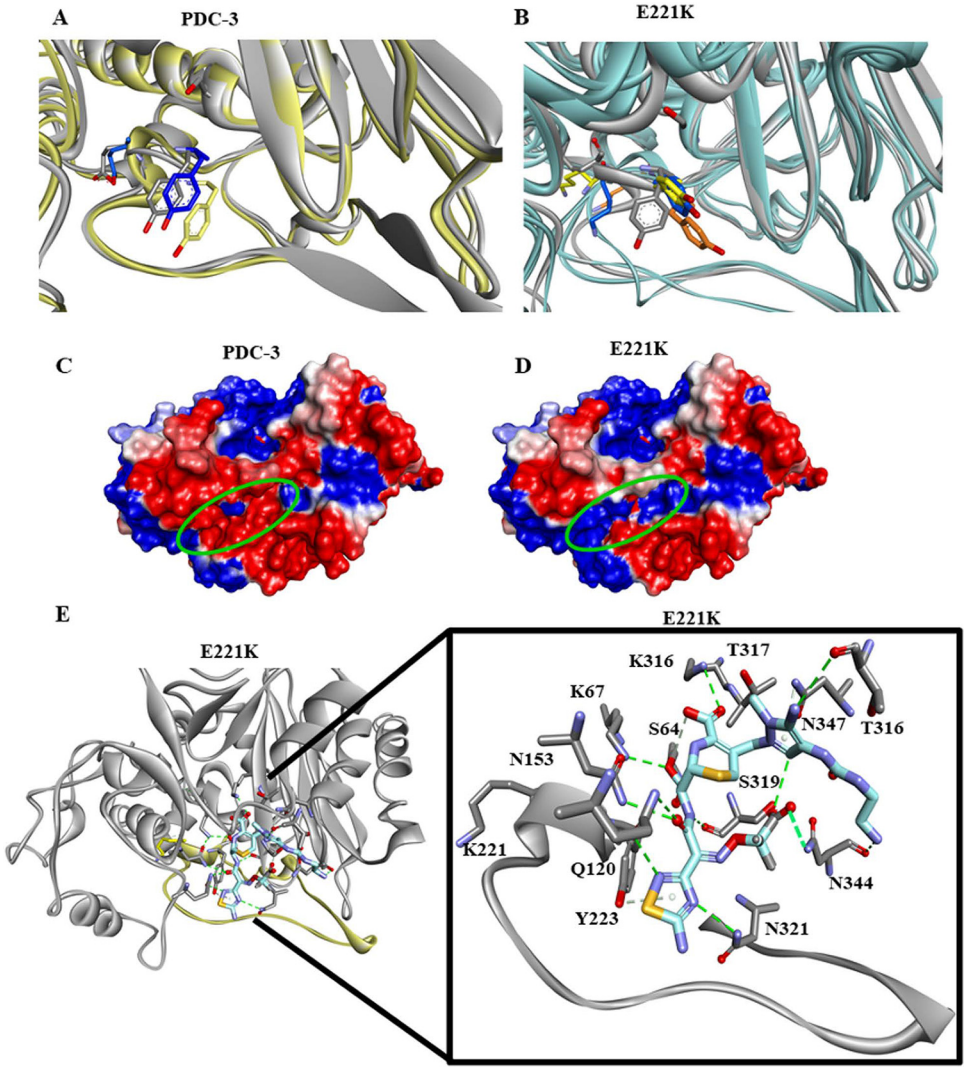

FIG 9 Representative conformations of PDC-3 (A) and E221K (B) corresponding to individual energetic basins extracted from metadynamics simulations which show the conformational change of Y223. Connolly representation of PDC-3 (C) and the E221K variant (D) based on the calculated electrostatic potential showing significant electrostatic changes introduced by the E221K substitution. (E) Molecular modeling of E221K and ceftolozane as acyl enzyme complex. Ceftolozane is represented as a stick figure with carbon in blue, sulfur in yellow, nitrogen in purple, and oxygen in red.

E221K variant at 1,304 kT (delta =13.4 kT). Docking of ceftolozane into the active site of the E221K variant illustrates that ceftolozane forms hydrogen bonds with residues S64, N153, K316, S319, K67, N344, and N321 (Fig. 9E). In addition, ceftolozane forms steric interactions with Y223, S319, and N347.

An accurate acyl-enzyme model of ceftolozane and PDC-3 was not possible because ceftolozane is too bulky to readily position into the active site of PDC-3. Ceftolozane sterically clashes with the active site residues at the entrance of PDC-3 (positions 120 to 125) and Ω-loop residues (positions 209 to 217), giving rise to a multitude of unproductive conformations. To better understand the effect of the single amino acid substitutions at an atomic level, we analyzed the dynamics and energetics of the PDC-3 and the E221K variant.

Enhanced sampling simulations reveal that the ion-pair interactions made between D191 and K226 help anchor the Ω-loop in a conformation that allows the side chain of Y223 to change its orientation to point away from the catalytic site. This in turn reveals a hidden pocket, which can accommodate the tail of ceftolozane. The increase in

conformational flexibility and expansion of the active site entrance likely explains why the E221K variant acquires the ability to accommodate ceftolozane in its active site and hydrolyze both ceftolozane and ceftazidime, despite the difference in size (Fig. 2).

Conclusions. Our previous findings showed that amino acid substitutions in the C_3/C_4 β-lactam carboxylate recognition region of PDC-3 increase or maintain antibiotic susceptibility (20). The emergence of mutations in AmpC β-lactamases as a mechanism of resistance to ceftolozane has gone largely unexplored (from a biochemical and mechanistic standpoint) with an underestimated occurrence of ≥1.5% resistance to β-lactams (12), but it has attracted more attention in recent years (11, 12, 34, 35). Here, we focused on clinically important amino acid substitutions in the Ω-loop of PDC-3 and how they contribute to the resistance profile. While PDC-3 is our primary focus in this study, the vital impact that the residues in the Ω-loop have on structural integrity and catalytic activity is not limited to PDC-3, or even class C, β-lactamases (22, 36–41). Herein, we first showed that the hydrolysis of ceftazidime by the wild-type β-lactamase PDC-3 is deficient despite the ability of ceftazidime to dwell in the active site of PDC-3. To our knowledge, this insight has not been significantly appreciated. A single amino acid substitution, E221K, in PDC-3 enabled the β-lactamase to acquire increased hydrolytic activity and induced multiple conformations of the variant, identified by enhanced sampling simulations. This particular substitution has already evolved in the clinic in multiple species (12, 14), and therefore may be evolutionarily favored to emerge in additional drug-resistant pathogens. The potential severity of the variants in the clinic is exacerbated by increased resistance to aztreonam as well as ceftolozane and ceftazidime. Further, employment of molecular dynamic simulations and other biophysical methods to capture dynamic interactions are useful for elucidating protein structure-function relationships.

The gain of function observed in enhanced catalysis is not obtained without a sacrifice. The E221K protein acquires hydrolytic activity at the detriment of conformational restraints that destabilize the infrastructure of the protein, which is partially restored by binding to inhibitors. Importantly, despite the E221K variant's enhanced cephalosporinase activity, avibactam and the LP-06 BATSI effectively lowered ceftolozane and ceftazidime MIC values of the E221K strain. BATSIs and DBOs may be able to serve as partners for novel combinational therapies against *P. aeruginosa* infections. More importantly, by differing significantly from the ceftolozane-tazobactam mechanism of inactivation, these "second-generation" β-lactamase inhibitors offer promise against this significant threat to our armamentarium (42).

MATERIALS AND METHODS

Critical reagents and strains. Ceftazidime was procured from Sigma-Aldrich (catalog no. C3809) and Research Products International (catalog no. 33527) and used interchangeably throughout the experimentation. Merck & Co., Inc. (Kenilworth, NJ, USA) provided ceftolozane powder. Avibactam was purchased from Advanced ChemBlocks (catalog no. R16073). Piperacillin (catalog no. P8396), cefotaxime (catalog no. C7912), and chloramphenicol (catalog no. R4405) were purchased from Sigma-Aldrich. Imipenem was obtained from USP (catalog no. 1337809) and from the commercial source. Tazobactam (catalog no. 15141) and aztreonam (catalog no. 15151) were purchased from Chem-Impex International. Ceftolozane-tazobactam, cefepime, and meropenem were obtained from their commercial sources. Nitrocefin (catalog no. BR0063G) was purchased from Oxoid. The LP-06 and S02030 BATSIs were synthesized as previously described (43, 44). See Drawz et al. (20) for a discussion on the *P. aeruginosa* control strains (18SH AmpC for PDC-3 and PAO1 for PDC-1).

Expression and purification of PDC-3 and E221K. PDC-3 β-lactamase was cloned into the pER24a (+) vector as previously described (20). PDC-3 β-lactamase was purified from *E. coli* Origami 2 DE3 (Novagen) cells carrying the pET24a (+) bla_{PDC-3} or pET24a (+) $bla_{PDC-3-E221K}$ plasmid that produces the corresponding PDC-3 protein without its signal peptide, similar to the previously described protocol (20, 45). Cells were grown in 500 ml super optimal broth (SOB) at 37°C to an optical density at 600 nm (OD_{600}) of approximately 0.6 to 0.8 and induced with 1 mM isopropyl-β-D-1-thiogalactopyranoside (IPTG) for a minimum of two and a half hours to express the β-lactamase. The cell pellets were generated by centrifugation and frozen at −20°C for ≥12 h prior to a 40-min lysis in 50 mM Tris-HCl buffer (pH 7.4) containing 40 mg/ml lysozyme, 0.1 mM magnesium sulfate, 250 U benzonase nuclease, and 1 mM ethylenediaminetetraacetic acid (EDTA). The supernatant was further purified using a HiTrap SP Sepharose cation exchange column (GE Healthcare Life Sciences) and 25 mM Tris-HCl (pH 7.4). Protein was eluted from the column using 25 mM Tris-HCl (pH 7.4) and 0.5 M NaCl. If needed, the sample of protein was concentrated using centrifugal filter units with a 10,000-dalton-molecular-weight cutoff (Millipore).

The protein was subjected to gel filtration using a Sepahadex (75 prep grade) HiLoad 16/600 column in 10 mM phosphate-buffered saline (PBS), pH 7.4. The final sample of protein was concentrated using centrifugal filter units with a 10,000-dalton-molecular-weight cutoff (Millipore). The purity of the proteins was assessed by quadrupole time of flight (Q-TOF) mass spectrometry (see below). Protein concentrations were determined by measuring absorbance at a wavelength of 280 nm (λ_{280}) and using the protein's extinction coefficient ($\Delta\varepsilon = 54{,}320\ M^{-1}\ cm^{-1}$) obtained using the ProtParam tool at ExPASy Bioinformatics Resource Portal.

Purification of anti-PDC-3 antibody. For the SPOTS membrane, the PDC-3 protein (3 mg of protein in 10 mM phosphate-buffered saline [PBS], pH 7.4) was provided to New England Peptide (Gardner, MA) for polyclonal antibody production in a rabbit. The serum was purified using a protein G column to obtain polyclonal immunoglobulin antibodies against PDC-3. Briefly, 3 ml of rabbit serum was added to a binding buffer composed of 20 mM NaH_2PO_4 (pH 7.0) and added to a 5-ml HiTrap Protein G HP column (GE Healthcare, Piscataway, NJ) with a flow rate of 0.5 ml/min. The bound anti-PDC-3 was eluted from the column using 0.1 M glycine-HCl (pH 2.7) and neutralized with 1 M Tris-HCl (pH 9.0). The antibody concentration was quantified using spectrophotometric determination at 280 nm and stored at −20°C.

Epitope mapping (SPOTs membrane). An epitope map of the PDC-3 β-lactamase was created using SPOT synthesis on a cellulose membrane by JPT Peptide Technologies GmbH (Berlin, Germany) as previously described (46, 47). Briefly, peptides with an acetylated N terminus were covalently bound to a Whatman 50 cellulose membrane by the C terminus. The membrane was incubated in methanol for 5 min, washed three times with Tris-buffered saline (TBS) for 10 min each time, and blocked with 5% milk in TBS overnight. The following day, the membrane was washed four times with TBS for 4 min each time. Primary antibody was added at 1 mg/liter in 5% milk in TBS for 3 h. Blots were washed four times with TBS-Tween (TBS-T) for 10 min each time before incubation with a secondary antibody (protein G-HRP) diluted 1:5,000 for 1 h. Blots were washed four times with TBS-T for 10 min each time and processed with the ECL Prime kit (Amersham/GE Healthcare, Piscataway, NJ).

Immunoblotting of PDC-3 β-lactamase. Log-phase protein expression was determined as previously described (45). One milliliter of bacteria grown to an OD_{600} of 0.6 to 0.8 in lysogeny broth (LB) in 20 μg/liter chloramphenicol was pelleted and resuspended in sodium dodecyl sulfate-polyacrylamide gel electrophoresis (SDS-PAGE) buffer. Each sample (10 μl) was separated by SDS-PAGE. Proteins were transferred to polyvinylidene fluoride membranes for 2 h at 80 V. The membranes were blocked overnight in 5% milk in Tris-buffered saline (TBS) solution, followed by a 1- to 3-h incubation with a 0.1 mg/liter primary PDC-3 (anti-18SH, 42) rabbit polyclonal antibody and an anti-DnaK rabbit polyclonal antibody (Stressgene, San Diego, CA) diluted 1:15,000 (loading control) in 5% milk/TBS and finally incubated with the protein G-HRP conjugate at a 1:10,000 dilution for 1 h in 5% milk/TBS. An ECL Prime Western blot exposure kit from Amersham was used to visualize the blot on the Fotodyne imager.

Susceptibility testing. Variant genes were synthesized into the pBC SK (-) vector by Celtek Bioscience (Franklin, TN). Mueller-Hinton (MH) agar-dilution MIC measurements were performed against isogenic transformants producing PDC-3 and nine variants of PDC-3 in pBC SK (-) according to the Clinical and Laboratory Standards Institute (CLSI) guidelines as previously described (39, 48). Avibactam, LP-06, and S02030 were tested at a constant 4 μg/ml in combination with various concentrations of ceftazidime. Piperacillin-tazobactam was maintained at a ratio of 8 piperacillin to 1 tazobactam. Ceftolozane-tazobactam was maintained at a ratio of 2 ceftolozane to 1 tazobactam. The MICs are reported as the concentrations at which bacterial growth was no longer observed. All MIC measurements were performed at least three times.

Steady-state kinetic and inhibitor analysis. Steady-state kinetic and inhibitor parameters were determined by using an Agilent 8453 diode array spectrophotometer at room temperature as previously described (20, 43, 49). Each assay was performed in 10 mM phosphate-buffered saline (PBS) at pH 7.4 at room temperature (RT = ~25°C) in a quartz cuvette with a 1-cm path length. Measurements were obtained using ceftolozane and ceftazidime. The kinetic parameters, V_{max} and K_m, were obtained with a nonlinear least-squares fit of the data (Henri Michaelis-Menten, equation 1) using Origin 7.5VR (OriginLab, Northampton, MA).

$$v = \frac{V_{\max}[S]}{K_m + [S]} \quad (1)$$

For the reversible boronic acid inhibitors, measurements were obtained for E221K and PDC-3 using nitrocefin ($\Delta\varepsilon 482 = 17{,}400\ M^{-1}\ cm^{-1}$) as a reporter substrate. Because of the time-dependent inhibition observed previously with some of the chiral boronates (43), the BATSIs were preincubated with enzyme for 5 min in phosphate-buffered saline before initiation of the reaction with the addition of substrate. The initial velocity (0 to 10 s) was measured in the presence of a constant concentration of enzyme (1.5 nM PDC-3 and 20 nM E221K) and increasing concentrations of the inhibitors against the fixed concentration (100 μM) of the indicator substrate, nitrocefin. The IC_{50} is the concentration of inhibitor that reduces the velocity by 50%. IC_{50} values were determined by fitting the initial velocity (v_o) measurements to equation 2.

$$v_0 = \frac{V_{\max}[S]}{K_m\left[1 + \frac{I}{IC_{50}}\right] + [S]} \quad (2)$$

For competitive inhibition assays used to determine $K_{i\ app}$, 150 μM nitrocefin was used as the reporter substrate with increasing concentrations of ceftazidime or ceftolozane. Initial velocities were plotted against concentrations of ceftazidime or ceftolozane. $K_{i\ app\ obs}$ were determined by dividing the slope by

the *y* intercept. $K_{i\ app}$ was calculated by correcting $K_{i\ app\ obs}$ for nitrocefin affinity and concentration (equation 3).

$$K_{i\,app} = K_{i\,app\,obs}/[1 + ([NCF]/K_{m\,NCF}) \quad (3)$$

Electrospray ionization mass spectrometry (ESI-MS). Five micrograms of β-lactamase (PDC-3, E221K) was incubated with the substrate at a 1:1 molar ratio (PDC-3 and ceftazidime or ceftolozane) in 10 mM PBS at pH 7.4 for a total reaction volume of 20 μl for the times indicated in the figures. Reactions were quenched with 10 μl acetonitrile and added to 1 ml of 0.1% formic acid in water. Samples were analyzed using Q-TOF Waters Synapt-G2-Si and Waters Acquity UPLC BEH C_{18} 1.7-μm column (2.1 by 50 mm). MassLynx V4.1 was used to deconvolute protein peaks. The tune settings for each data run were as follows: capillary voltage at 3.5 kV, sampling cone at 35, source offset at 35, source temperature of 100°C, desolvation temperature of 500°C, cone gas at 100 liters/h, desolvation gas at 800 liters/h, and nebulizer bar at 6.0. Mobile phase A was 0.1% formic acid in water. Mobile phase B was 0.1% formic acid in acetonitrile. The mass accuracy of this system is ±5 Da.

Thermal denaturation. Circular dichroism (CD) experiments were carried out in a Jasco (Easton, MD) J-815 spectrometer with a Peltier effect temperature controller. Quartz cells with a 0.1-cm path length were used for all experiments.

PDC-3 enzyme and the E221K variant (10 μM) with or without S02030 or LP-06 (200 μM) were monitored for thermal denaturation by CD at λ_{215} and λ_{221} between 20 and 80°C with a heating rate of 2°C/min. Two-state behavior was indicated by identical curves at each wavelength. Raw equilibrium denaturation data were normalized to the fraction of denatured protein (f_U). With the assumption of a reversible two-state transition (N ↔ U), equilibrium constants (K_{eq}) at any given temperature were calculated, as previously described (32), using equation 4

$$K_{eq} = f_U/(1 - f_U) \quad (4)$$

With the assumption that enthalpy and entropy changes do not vary with the temperature (ΔC_p = constant), from the Gibbs free energy and van't Hoff equation ($\Delta G = \Delta H_{VH} - T\Delta S = -RT\ln K_{eq}$) (50) the ΔH_{VH} was determined as the slope from equation 5 (R is the gas constant). The melting temperature T_m was determined at the midpoint of equilibrium folding ($T = T_m$) when $\Delta G = 0$.

$$\ln K_{eq} = 1/T\,(-\Delta H/R) + \Delta S/R \quad (5)$$

The free energy of unfolding was determined as previously described using the equation $\Delta\Delta G_u = \Delta T_m \Delta S_u^{PDC\text{-}3}$ (Schellman), where $\Delta S_u^{PDC\text{-}3} = 0.326 \pm 0.02$ Kcal mol^{-1} K^{-1}.

Molecular modeling. (i) Docking. Structural representations of PDC-3 and the E221K variant of KPC-2 β-lactamase were generated using the crystal coordinates of *P. aeruginosa* AmpC (PDC-1) (PDB ID 4HEF) and Discovery Studio 2016 (DS 2016) (Dassault Systèmes BIOVIA; Discovery Studio Modeling Environment, San Diego, CA) molecular modeling software as previously described (37, 51). The T79A substitution (T79A substitution corresponds to T105A in 4HEF because of the 26-amino-acid signal peptide) was incorporated into the PDC-1 β-lactamase structure to obtain the PDC-3 β-lactamase structure.

(ii) Acyl complex. The PDC-3 β-lactamase structure and the variant model were solvated and minimized to an RMS of 0.03 Å using the conjugate gradient method. The intact and acylated ceftolozane were constructed using the Fragment Builder tools and minimized using a Standard Dynamics Cascade protocol of DS. Both molecules were docked automatically into the active site of the PDC-3 and E221K variant using CDOCKER module of DS. To obtain acyl-enzyme complexes, the most favorable conformation demonstrating anticipated active site contacts was chosen, and the complex was further minimized. The spatial distribution of the electrostatic potential and the potential of PDC-3 and E221K variant atoms were calculated using the DelPhi program with Debye-Huckel boundary condition approximation. The DelPhi calculation was based on a two-dielectric implicit solvent model and a finite difference method to solve the Poisson-Boltzmann equation on a cubic grid (52, 53).

Classical molecular dynamics and well-tempered metadynamics. The structure of the PDC-3 β-lactamase was prepared starting from the Protein Data Bank (PDB ID 4HEF) (54) with a T79A substitution. Nine variants (V213A, V213G, G216A, G216R, E221A, E221G, E221K, Y223A, and Y223H) were constructed *in silico* using the ICM mutagenesis program (55). The system was prepared using a high-throughput molecular dynamics (HTMD) protocol (56). Amberff14SB force field was used to define the parameters of the protein (57), combined with explicit TIP3P water molecules (58). The systems were minimized with 1,000 steps of steepest descent integrator and equilibrated in the NPT ensemble for 5 ns, using a Berendsen barostat at 1 atm (59). The temperature was kept at 300 K° by a Langevin thermostat. A 550-ns production run was carried out for all the systems in the NVT ensemble with a time step of 4 fs. All the simulations were carried out with the ACEMD program (60). To enhance sampling, Well-Tempered Metadynamics simulations (61, 62) (WTMetaD) starting from the equilibrated structures of the wild-type PDC-3 and variant structures were performed at 300 K using the software ACEMD and the PLUMED 1.3 plug-in using an integration step of 4 fs. To study the flexibility of the Ω-loop as a function of the variants, we chose the dihedral angles of the WT/variant residue to be the collective variable (CV). The choice of the CVs (CV1 = ϕ and CV2 = ϕ of the substituted residue) was based on the observation that the slowest motions in a protein are a function of their backbone flexibility (63). Therefore, the differences in the structural effects resulting from the changes between the wild type and the variants should be pronounced in the backbone dihedral angles. The bias was added on the two CVs by setting Gaussian width of 0.1 and 0.1 rad, respectively, while the Gaussian height was at 0.5 kJ/mol. Gaussians were deposited every 4 ps, so that the deposition rate was equal to 0.125 kJ/(mol·ps). The bias factor was fixed to 15. A total of 550 ns in the NVT ensemble were needed to reach full convergence of the free

energy (see Fig. S2 in the supplemental material). The free energy surface of the WTMetaD simulation as a function of the two CVs is readily obtained by integrating the deposited energy bias along the trajectory. The error on the minima and barriers of the free energy surface was estimated from the largest variation observed in the monodimensional projections along the collective variables during the last 100 ns of the simulation. It amounts to 0.5 kcal/mol.

The structures corresponding to the minima were selected from the WTMetaD trajectories based on the values of the collective variables CV1 and CV2. The RMSF of the Ω-loop was calculated from the unbiased simulations of 1,000 ns of the WT and mutants, using the g_rmsf tool of the GROMACS 5.1.4 package (64). To remove the effect of slow, large-scale conformational transitions, the RMSF was calculated on the Cα atoms in overlapping windows of 100 ns each and averaged afterwards. The first 150 ns of the simulation were considered equilibration time and omitted from the calculation. The structural figures were generated using VMD and ICM-Pro software (55, 65, 66).

SUPPLEMENTAL MATERIAL

Supplemental material for this article may be found at https://doi.org/10.1128/mBio.02085-18.

FIG S1, TIF file, 1.9 MB.

FIG S2, TIF file, 2.6 MB.

ACKNOWLEDGMENTS

Merck & Co., Inc. (Kenilworth, NJ, USA) provided ceftolozane powder for this study.

This research was supported by funds and/or facilities provided by the Cleveland Department of Veterans Affairs to K.M.P.-W. and R.A.B., the Veterans Affairs Merit Review Program award 1I01BX002872 to K.M.P.-W. and the Veterans Affairs Merit Review Program award 1I01BX001974 to R.A.B. from the Biomedical Laboratory Research & Development Service of the VA Office of Research and Development and the Geriatric Research Education and Clinical Center VISN 10. R.A.B. is also supported by the National Institute of Allergy and Infectious Diseases of the National Institutes of Health by awards R01AI100560, R01AI063517, and R01AI072219.

The content is solely the responsibility of the authors and does not necessarily represent the official views of the National Institutes of Health, the U.S. Department of Veterans Affairs, or the U.S. Government.

REFERENCES

1. Centers for Disease Control and Prevention. 2013. Antibiotic resistance threats in the United States, 2013. Centers for Disease Control and Prevention, Atlanta, GA. http://www.cdc.gov/drugresistance/threat-report-2013/index.html.
2. World Health Organization. 2017. Guidelines for the prevention and control of carbapenem-resistant Enterobacteriaceae, *Acinetobacter baumannii* and *Pseudomonas aeruginosa* in health care facilities. World Health Organization, Geneva, Switzerland.
3. Weiner LM, Webb AK, Limbago B, Dudeck MA, Patel J, Kallen AJ, Edwards JR, Sievert DM. 2016. Antimicrobial-resistant pathogens associated with healthcare-associated infections: summary of data reported to the National Healthcare Safety Network at the Centers for Disease Control and Prevention, 2011-2014. Infect Control Hosp Epidemiol 37:1288–1301. https://doi.org/10.1017/ice.2016.174.
4. Takeda S, Ishii Y, Hatano K, Tateda K, Yamaguchi K. 2007. Stability of against AmpC β-lactamase of *Pseudomonas aeruginosa*. Int J Antimicrob Agents 30:443–445. https://doi.org/10.1016/j.ijantimicag.2007.05.019.
5. Bush K, Page MG. 2017. What we may expect from novel antibacterial agents in the pipeline with respect to resistance and pharmacodynamic principles. J Pharmacokinet Pharmacodyn 44:113–132. https://doi.org/10.1007/s10928-017-9506-4.
6. Gangcuangco LM, Clark P, Stewart C, Miljkovic G, Saul ZK. 2016. Persistent bacteremia from *Pseudomonas aeruginosa* with in vitro resistance to the novel antibiotics ceftolozane-tazobactam and ceftazidime-avibactam. Case Rep Infect Dis 2016:1520404. https://doi.org/10.1155/2016/1520404.
7. Munita JM, Aitken SL, Miller WR, Perez F, Rosa R, Shimose LA, Lichtenberger PN, Abbo LM, Jain R, Nigo M, Wanger A, Araos R, Tran TT, Adachi J, Rakita R, Shelburne S, Bonomo RA, Arias CA. 2017. Multicenter evaluation of ceftolozane/tazobactam for serious infections caused by carbapenem-resistant Pseudomonas aeruginosa. Clin Infect Dis 65:158–161.
8. Fraile-Ribot PA, Cabot G, Mulet X, Perianez L, Martin-Pena ML, Juan C, Perez JL, Oliver A. 2017. Mechanisms leading to in vivo ceftolozane/tazobactam resistance development during the treatment of infections caused by MDR Pseudomonas aeruginosa. J Antimicrob Chemother 73:658–663. https://doi.org/10.1093/jac/dkx424.
9. Jacoby GA. 2009. AmpC β-lactamases. Clin Microbiol Rev 22:161–182. https://doi.org/10.1128/CMR.00036-08.
10. Nordmann P, Mammeri H. 2007. Extended-spectrum cephalosporinases: structure, detection and epidemiology. Future Microbiol 2:297–307. https://doi.org/10.2217/17460913.2.3.297.
11. Cabot G, Bruchmann S, Mulet X, Zamorano L, Moya B, Juan C, Haussler S, Oliver A. 2014. *Pseudomonas aeruginosa* ceftolozane-tazobactam resistance development requires multiple mutations leading to overexpression and structural modification of AmpC. Antimicrob Agents Chemother 58:3091–3099. https://doi.org/10.1128/AAC.02462-13.
12. Berrazeg M, Jeannot K, Ntsogo Enguéné VY, Broutin I, Loeffert S, Fournier D, Plésiat P. 2015. Mutations in β-lactamase AmpC increase resistance of *Pseudomonas aeruginosa* isolates to antipseudomonal cephalosporins. Antimicrob Agents Chemother 59:6248–6255. https://doi.org/10.1128/AAC.00825-15.
13. Lahiri SD, Walkup GK, Whiteaker JD, Palmer T, McCormack K, Tanudra MA, Nash TJ, Thresher J, Johnstone MR, Hajec L, Livchak S, McLaughlin RE, Alm RA. 2015. Selection and molecular characterization of ceftazidime/avibactam-resistant mutants in *Pseudomonas aeruginosa* strains containing derepressed AmpC. J Antimicrob Chemother 70:1650–1658. https://doi.org/10.1093/jac/dkv004.
14. Matsumura N, Minami S, Mitsuhashi S. 1998. Sequences of homologous β-lactamases from clinical isolates of *Serratia marcescens* with different substrate specificities. Antimicrob Agents Chemother 42:176–179.
15. Zasowski EJ, Rybak JM, Rybak MJ. 2015. The β-lactams strike back:

ceftazidime-avibactam. Pharmacotherapy 35:755–770. https://doi.org/10.1002/phar.1622.
16. Ehmann DE, Jahic H, Ross PL, Gu RF, Hu J, Kern G, Walkup GK, Fisher SL. 2012. Avibactam is a covalent, reversible, non-β-lactam β-lactamase inhibitor. Proc Natl Acad Sci U S A 109:11663–11668. https://doi.org/10.1073/pnas.1205073109.
17. Rojas LJ, Taracila MA, Papp-Wallace KM, Bethel CR, Caselli E, Romagnoli C, Winkler ML, Spellberg B, Prati F, Bonomo RA. 2016. Boronic acid transition state inhibitors active against KPC and other class A β-lactamases: structure-activity relationships as a guide to inhibitor design. Antimicrob Agents Chemother 60:1751–1759. https://doi.org/10.1128/AAC.02641-15.
18. Kurz SG, Hazra S, Bethel CR, Romagnoli C, Caselli E, Prati F, Blanchard JS, Bonomo RA. 2015. Inhibiting the β-lactamase of Mycobacterium tuberculosis (Mtb) with novel boronic acid transition-state inhibitors (BATSIs). ACS Infect Dis 1:234–242. https://doi.org/10.1021/acsinfecdis.5b00003.
19. Gutierrez O, Juan C, Cercenado E, Navarro F, Bouza E, Coll P, Perez JL, Oliver A. 2007. Molecular epidemiology and mechanisms of carbapenem resistance in *Pseudomonas aeruginosa* isolates from Spanish hospitals. Antimicrob Agents Chemother 51:4329–4335. https://doi.org/10.1128/AAC.00810-07.
20. Drawz SM, Taracila M, Caselli E, Prati F, Bonomo RA. 2011. Exploring sequence requirements for C_3/C_4 carboxylate recognition in the *Pseudomonas aeruginosa* cephalosporinase: insights into plasticity of the AmpC β-lactamase. Protein Sci 20:941–958. https://doi.org/10.1002/pro.612.
21. Perez-Inestrosa E, Suau R, Montanez MI, Rodriguez R, Mayorga C, Torres MJ, Blanca M. 2005. Cephalosporin chemical reactivity and its immunological implications. Curr Opin Allergy Clin Immunol 5:323–330.
22. Barnes MD, Winkler ML, Taracila MA, Page MG, Desarbre E, Kreiswirth BN, Shields RK, Nguyen MH, Clancy C, Spellberg B, Papp-Wallace KM, Bonomo RA. 2017. *Klebsiella pneumoniae* carbapenemase-2 (KPC-2), substitutions at Ambler position Asp179, and resistance to ceftazidime-avibactam: unique antibiotic-resistant phenotypes emerge from β-lactamase protein engineering. mBio 8:e00528-17. https://doi.org/10.1128/mBio.00528-17.
23. Faraci WS, Pratt RF. 1985. Mechanism of inhibition of the PC1 β-lactamase of *Staphylococcus aureus* by cephalosporins: importance of the 3′-leaving group. Biochemistry 24:903–910.
24. Faraci WS, Pratt RF. 1984. Elimination of a good leaving group from the 3′-position of a cephalosporin need not be concerted with β-lactam ring opening: TEM-2 β-lactamase-catalyzed hydrolysis of pyridine-2-azo-4′-(N′,N′-dimethylaniline) cephalosporin (PADAC) and of cephaloridine. J Am Chem Soc 106:1489–1490. https://doi.org/10.1021/ja00317a053.
25. Drawz SM, Bonomo RA. 2010. Three decades of β-lactamase inhibitors. Clin Microbiol Rev 23:160–201. https://doi.org/10.1128/CMR.00037-09.
26. Toda A, Ohki H, Yamanaka T, Murano K, Okuda S, Kawabata K, Hatano K, Matsuda K, Misumi K, Itoh K, Satoh K, Inoue S. 2008. Synthesis and SAR of novel parenteral anti-pseudomonal cephalosporins: discovery of. Bioorg Med Chem Lett 18:4849–4852. https://doi.org/10.1016/j.bmcl.2008.07.085.
27. Laws A, Page M. 1996. The chemistry and structure-activity relationships of C3-quaternary ammonium cephem antibiotics. J Chemother 8:7–22.
28. Rodriguez-Martinez JM, Poirel L, Nordmann P. 2009. Extended-spectrum cephalosporinases in *Pseudomonas aeruginosa*. Antimicrob Agents Chemother 53:1766–1771. https://doi.org/10.1128/AAC.01410-08.
29. Winkler ML, Rodkey EA, Taracila MA, Drawz SM, Bethel CR, Papp-Wallace KM, Smith KM, Xu Y, Dwulit-Smith JR, Romagnoli C, Caselli E, Prati F, van den Akker F, Bonomo RA. 2013. Design and exploration of novel boronic acid inhibitors reveals important interactions with a clavulanic acid-resistant sulfhydryl-variable (SHV) β-lactamase. J Med Chem 56:1084–1097. https://doi.org/10.1021/jm301490d.
30. Caselli E, Romagnoli C, Powers RA, Taracila MA, Bouza AA, Swanson HC, Smolen KA, Fini F, Wallar BJ, Bonomo RA, Prati F. 2018. Inhibition of Acinetobacter-derived cephalosporinase: exploring the carboxylate recognition site using novel β-lactamase inhibitors. ACS Infect Dis 4:337–348. https://doi.org/10.1021/acsinfecdis.7b00153.
31. Beadle BM, McGovern SL, Patera A, Shoichet BK. 1999. Functional analyses of AmpC β-lactamase through differential stability. Protein Sci 8:1816–1824. https://doi.org/10.1110/ps.8.9.1816.
32. Bouza AA, Swanson HC, Smolen KA, VanDine AL, Taracila MA, Romagnoli C, Caselli E, Prati F, Bonomo RA, Powers RA, Wallar BJ. 2018. Structure-based analysis of boronic acids as inhibitors of Acinetobacter-derived cephalosporinase-7, a unique class C β-lactamase. ACS Infect Dis 4:325–336. https://doi.org/10.1021/acsinfecdis.7b00152.
33. Thomas VL, McReynolds AC, Shoichet BK. 2010. Structural bases for stability-function tradeoffs in antibiotic resistance. J Mol Biol 396:47–59. https://doi.org/10.1016/j.jmb.2009.11.005.
34. Haidar G, Philips NJ, Shields RK, Snyder D, Cheng S, Potoski BA, Doi Y, Hao B, Press EG, Cooper VS, Clancy CJ, Nguyen MH. 2017. Ceftolozane-tazobactam for the treatment of multidrug-resistant *Pseudomonas aeruginosa* infections: clinical effectiveness and evolution of resistance. Clin Infect Dis 65:110–120. https://doi.org/10.1093/cid/cix182.
35. MacVane SH, Pandey R, Steed LL, Kreiswirth BN, Chen L. 2017. Emergence of ceftolozane-tazobactam-resistant *Pseudomonas aeruginosa* during treatment is mediated by a single AmpC structural mutation. Antimicrob Agents Chemother 61:e01183-17. https://doi.org/10.1128/AAC.01183-17.
36. Sampson JM, Ke W, Bethel CR, Pagadala SR, Nottingham MD, Bonomo RA, Buynak JD, van den Akker F. 2011. Ligand-dependent disorder of the Omega loop observed in extended-spectrum SHV-type β-lactamase. Antimicrob Agents Chemother 55:2303–2309. https://doi.org/10.1128/AAC.01360-10.
37. Levitt PS, Papp-Wallace KM, Taracila MA, Hujer AM, Winkler ML, Smith KM, Xu Y, Harris ME, Bonomo RA. 2012. Exploring the role of a conserved class A residue in the omega-loop of KPC-2 β-lactamase: a mechanism for ceftazidime hydrolysis. J Biol Chem 287:31783–31793. https://doi.org/10.1074/jbc.M112.348540.
38. Becka SA, Zeiser ET, Barnes MD, Taracila MA, Nguyen K, Singh I, Sutton GG, LiPuma JJ, Fouts DE, Papp-Wallace KM. 2018. Characterization of the AmpC β-lactamase from *Burkholderia multivorans*. Antimicrob Agents Chemother 62:e01140-18. https://doi.org/10.1128/AAC.01140-18.
39. Winkler ML, Papp-Wallace KM, Bonomo RA. 2015. Activity of ceftazidime/avibactam against isogenic strains of *Escherichia coli* containing KPC and SHV β-lactamases with single amino acid substitutions in the omega-loop. J Antimicrob Chemother 70:2279–2286. https://doi.org/10.1093/jac/dkv094.
40. Banerjee S, Pieper U, Kapadia G, Pannell LK, Herzberg O. 1998. Role of the omega-loop in the activity, substrate specificity, and structure of class A β-lactamase. Biochemistry 37:3286–3296. https://doi.org/10.1021/bi972127f.
41. Petrosino JF, Palzkill T. 1996. Systematic mutagenesis of the active site omega loop of TEM-1 β-lactamase. J Bacteriol 178:1821–1828.
42. van Duin D, Bonomo RA. 2016. Ceftazidime/avibactam and ceftolozane/tazobactam: second-generation β-lactam/β-lactamase inhibitor combinations. Clin Infect Dis 63:234–241. https://doi.org/10.1093/cid/ciw243.
43. Caselli E, Romagnoli C, Vahabi R, Taracila MA, Bonomo RA, Prati F. 2015. Click chemistry in lead optimization of boronic acids as β-lactamase inhibitors. J Med Chem 58:5445–5458. https://doi.org/10.1021/acs.jmedchem.5b00341.
44. Prati F, Caselli E. 18 April 2013. Boronic acid inhibitors of β-lactamases. Patent no. WO2013053372.
45. Winkler ML, Papp-Wallace KM, Hujer AM, Domitrovic TN, Hujer KM, Hurless KN, Tuohy M, Hall G, Bonomo RA. 2015. Unexpected challenges in treating multidrug-resistant Gram-negative bacteria: resistance to ceftazidime-avibactam in archived isolates of *Pseudomonas aeruginosa*. Antimicrob Agents Chemother 59:1020–1029. https://doi.org/10.1128/AAC.04238-14.
46. Hujer AM, Page MG, Helfand MS, Yeiser B, Bonomo RA. 2002. Development of a sensitive and specific enzyme-linked immunosorbent assay for detecting and quantifying CMY-2 and SHV β-lactamases. J Clin Microbiol 40:1947–1957.
47. Papp-Wallace KM, Taracila M, Hornick JM, Hujer AM, Hujer KM, Distler AM, Endimiani A, Bonomo RA. 2010. Substrate selectivity and a novel role in inhibitor discrimination by residue 237 in the KPC-2 β-lactamase. Antimicrob Agents Chemother 54:2867–2877. https://doi.org/10.1128/AAC.00197-10.
48. Clinical and Laboratory Standards Institute. 2017. Performance standards for antimicrobial susceptibility testing; twenty-seventh informational supplement. Clinical and Laboratory Standards Institute, Wayne, PA.
49. Papp-Wallace KM, Winkler ML, Taracila MA, Bonomo RA. 2015. Variants of β-lactamase KPC-2 that are resistant to inhibition by avibactam. Antimicrob Agents Chemother 59:3710–3717. https://doi.org/10.1128/AAC.04406-14.
50. Greenfield NJ. 2007. Using circular dichroism collected as a function of temperature to determine the thermodynamics of protein unfolding and binding interactions. Nat Protoc 1:2527–2535. https://doi.org/10.1038/nprot.2006.204.

51. Papp-Wallace KM, Taracila MA, Smith KM, Xu Y, Bonomo RA. 2012. Understanding the molecular determinants of substrate and inhibitor specificities in the carbapenemase KPC-2: exploring the roles of Arg220 and Glu276. Antimicrob Agents Chemother 56:4428–4438. https://doi.org/10.1128/AAC.05769-11.
52. Rocchia W, Alexov E, Honig B. 2001. Extending the applicability of the nonlinear Poisson-Boltzmann equation: multiple dielectric constants and multivalent ions. J Phys Chem B 105:6507–6514. https://doi.org/10.1021/jp010454y.
53. Rocchia W, Sridharan S, Nicholls A, Alexov E, Chiabrera A, Honig B. 2002. Rapid grid-based construction of the molecular surface and the use of induced surface charge to calculate reaction field energies: applications to the molecular systems and geometric objects. J Comput Chem 23:128–137. https://doi.org/10.1002/jcc.1161.
54. Lahiri SD, Mangani S, Durand-Reville T, Benvenuti M, De Luca F, Sanyal G, Docquier JD. 2013. Structural insight into potent broad-spectrum inhibition with reversible recyclization mechanism: avibactam in complex with CTX-M-15 and *Pseudomonas aeruginosa* AmpC β-lactamases. Antimicrob Agents Chemother 57:2496–2505. https://doi.org/10.1128/AAC.02247-12.
55. Abagyan R, Totrov T, Kuznetsov D. 1994. ICM—a new method for protein modeling and design: applications to docking and structure prediction from the distorted native conformation. J Comput Chem 15:488–506. https://doi.org/10.1002/jcc.540150503.
56. Doerr S, Harvey MJ, Noe F, De Fabritiis G. 2016. HTMD: high-throughput molecular dynamics for molecular discovery. J Chem Theory Comput 12:1845–1852. https://doi.org/10.1021/acs.jctc.6b00049.
57. Case DA, Cheatham TE, III, Darden T, Gohlke H, Luo R, Merz KM, Jr, Onufriev A, Simmerling C, Wang B, Woods RJ. 2005. The Amber biomolecular simulation programs. J Comput Chem 26:1668–1688. https://doi.org/10.1002/jcc.20290.
58. Price DJ, Brooks CL, III. 2004. A modified TIP3P water potential for simulation with Ewald summation. J Chem Phys 121:10096–10103. https://doi.org/10.1063/1.1808117.
59. Berendsen HJC, Postma JPM, van Gunsteren WF, DiNola A, Haak JR. 1984. Molecular dynamics with coupling to an external bath. J Chem Phys 81:3684–3690. https://doi.org/10.1063/1.448118.
60. Harvey MJ, Giupponi G, Fabritiis GD. 2009. ACEMD: accelerating biomolecular dynamics in the microsecond time scale. J Chem Theory Comput 5:1632–1639. https://doi.org/10.1021/ct9000685.
61. Bonomi M, Barducci A, Parrinello M. 2009. Reconstructing the equilibrium Boltzmann distribution from well-tempered metadynamics. J Comput Chem 30:1615–1621. https://doi.org/10.1002/jcc.21305.
62. Laio A, Gervasio FL. 2008. Metadynamics: a method to simulate rare events and reconstruct the free energy in biophysics, chemistry, and material science. Rep Prog Phys 71:126601.
63. Skliros A, Zimmermann MT, Chakraborty D, Saraswathi S, Katebi AR, Leelananda SP, Kloczkowski A, Jernigan RL. 2012. The importance of slow motions for protein functional loops. Phys Biol 9:014001. https://doi.org/10.1088/1478-3975/9/1/014001.
64. Hess B, Kutzner C, van der Spoel D, Lindahl E. 2008. Algorithms for highly efficient, load-balanced, and scalable molecular simulation. J Chem Theory Comput 4:435–447. https://doi.org/10.1021/ct700301q.
65. DeLano WL. 2009. PyMOL molecular viewer: updates and refinements. Abstr Pap Am Chem Soc, abstr 238.
66. Humphrey W, Dalke A, Schulten K. 1996. VMD: visual molecular dynamics. J Mol Graph 14:33–38, 27–28. https://doi.org/10.1016/0263-7855(96)00018-5.